J|A|C|S
ARTICLES
Published on Web 07/16/2002

Switchable Electronic Coupling in Model Oligoporphyrin Molecular Wires Examined through the Measurement and Assignment of Electronic Absorption Spectra

Karina Sendt,[†] Lesley A. Johnston,[†] Warren A. Hough,[†] Maxwell J. Crossley,*[,†] Noel S. Hush,[†,‡] and Jeffrey R. Reimers*[,†]

Contribution from The School of Chemistry and The School of Molecular and Biomolecular Sciences, The University of Sydney, NSW 2006, Australia

Received January 16, 2002

Abstract: The use of a quinone functionality in the linkage unit of laterally bridged oligoporphyrins as a switch for controlling electronic coupling between the termini is examined. The quinone-bridged bisporphyrin $P_2TA\text{-}O_2$ was synthesized by condensation of 2 equiv of the dione 2,3-dioxo-5,10,15,20-tetrakis(3,5-di-*tert*-butylphenyl)chlorin with 2,3,5,6-tetraamino-1,4-benzoquinone. The electronic absorption spectra of $P_2TA\text{-}O_2$ and its conjugated benzenoid analogue P_2TA are measured and assigned, in conjunction with the spectra of the fragment monomers and porphyrin−bridge compounds. Band homologies and CASPT2 calculations are used to make the assignments. Chemically, the dimer in one case is bridged by a through-conjugated, π-delocalized 1,4,5,8-tetraazaanthracene molecule. This is shown to display significant inter-porphyrin coupling, with an observed *difference* in the exciton couplings of the B_x and B_y bands being ca. 0.18 eV. However, the other dimer is bridged using a derivative in which the central ring is converted to a cross-conjugated, π-localized quinonoid form; this molecule displays no observable inter-porphyrin coupling. This scenario provides a paradigm for the use of molecular electronic devices in sensing, control, and high-capacity relatively low-speed data storage applications.

1. Introduction

In recent years there has been considerable interest in the use of conjugated oligoporphyrins as molecular wires and molecular switches. To effectively transfer electronic charge over the length of the wire, the total end-to-end electronic coupling and hence the π delocalization over the length of the molecule are important.[1−7] Conversely, to effectively insulate against electronic communication between the end of the molecule, areas of π localization into single and double bonds are required. By controlling the π delocalization over a molecular wire, the conductor/insulator properties of the wire may be manipulated.[7]

Oligoporphyrin systems have been of particular interest for a variety of reasons,[7] ranging from relative ease of synthesis to the possibility of producing a variety of nanoelectronic components such as junctions, switches, and diodes. Many different porphyrin oligomers have been studied.[8] There are two different positions on the porphyrin molecule to which a bridging or linking molecule may be attached; these are the *meso* and the β-pyrrolic carbon atoms. While considerable attention has been focused on the *meso*-linked structures by others, we have been developing β-pyrrolic linked structures.[7,9−11] In particular, porphyrins linked by 1,4,5,8-tetraazaanthracene (TA) have been designed with the intent of producing a conductor, while a related quinonoidal form, 1,4,5,8-tetraaza-9,10-anthraquinone ($TA\text{-}O_2$), has been designed with the intent of producing an insulator. The π-delocalization in TA and the localization in $TA\text{-}O_2$ are apparent from the Lewis structures of these molecules; these are shown in Figure 1.

In this work, the electronic spectra of a substituted porphyrin P, this molecule with a single bridge molecule fused [P_1TA and $P_1TA\text{-}O_2$ as shown in Figure 1], and its dimers with each of the bridge molecules [P_2TA and $P_2TA\text{-}O_2$] are measured and then assigned using quantum chemical methods. Note that all of the experimental results presented refer to molecules with solubilizing groups [*meso*-tetrakis(3,5-di-*tert*-butylphenyl) for porphyrin, terminal methyl for anthracene, as detailed in Figure 1] while all calculations are for the unsubstituted parent

[†] The School of Chemistry.
[‡] The School of Molecular and Biomolecular Sciences.
* Address correspondence to these authors. E-mail: (J.R.R., regarding computation) Reimers@chem.usyd.edu.au; (M.J.C., regarding synthesis) Crossley@chem.usyd.edu.au.

(1) Reimers, J. R.; Hush, N. S. *Chem. Phys.* **1989**, *134*, 323.
(2) Reimers, J. R.; Hush, N. S. *J. Photochem. Photobiol., A* **1994**, *82*, 31.
(3) Lü, T. X.; Reimers, J. R.; Crossley, M. J.; Hush, N. S. *J. Phys. Chem.* **1994**, *98*, 11878.
(4) Reimers, J. R.; Lü, T. X.; Crossley, M. J.; Hush, N. S. *Chem. Phys. Lett.* **1996**, *256*, 353.
(5) Mujica, V.; Kemp, M.; Roitberg, A.; Ratner, M. A. *J. Chem. Phys.* **1996**, *104*, 7296.
(6) Hall, L. E.; Reimers, J. R.; Hush, N. S.; Silverbrook, K. *J. Chem. Phys.* **2000**, *112*, 1510.
(7) Hush, N. S.; Reimers, J. R.; Hall, L. E.; Johnston, L. A.; Crossley, M. J. *Ann. N. Y. Acad. Sci.* **1998**, *852*, 1.
(8) Anderson, H. L. *Chem. Commun.* **1999**, 2323.
(9) Crossley, M. J.; Burn, P. L. *J. Chem. Soc., Chem. Commun.* **1991**, 1569.
(10) Crossley, M. J.; Govenlock, L. J.; Prashar, J. K. *J. Chem. Soc., Chem. Commun.* **1995**, 2379.
(11) Reimers, J. R.; Hall, L. E.; Crossley, M. J.; Hush, N. S. *J. Phys. Chem. A* **1999**, *103*, 4385.

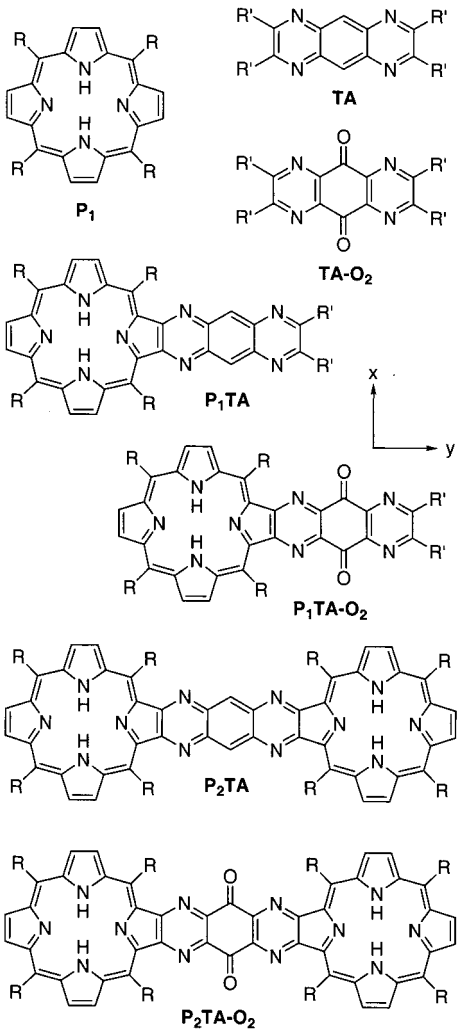

Figure 1. Lewis structures and axis conventions of the oligoporphyrin dimers P_2TA and $P_2TA\text{-}O_2$ as well as their fragment molecules P_1, TA, $TA\text{-}O_2$, and porphyrin−bridge compounds P_1TA and $P_1TA\text{-}O_2$. Experiment: R = 3,5-di-*tert*-butylphenyl and R′ = CH_3. Calculations: R = H and R′ = H.

compounds. The primary aim is, on the basis of the band assignments, to determine the magnitude of the electronic coupling between the porphyrin molecules in the dimers and hence verify that the bridges do indeed have the desired electronic properties. By developing related molecules which facilitate the interconversion of bridges with quinonoidal and benzenoidal forms, a chemically controllable, reversible, molecular switch unit could be built; our compounds thus form a model system, demonstrating a new paradigm for molecular electronic devices.

The electronic spectrum of porphyrins such as P, shown in Figure 2, is dominated by two low-energy, low-intensity transitions known as the Q bands, and two very intense high-energy transitions known as the Soret or B bands. For the Q bands, the lower energy transition is polarized along the axis containing the hydrogen atoms, which is taken to be the *x*-axis, with the higher energy (and more intense) transition polarized along the *y*-axis. The Q bands are the only ones with observable vibrational structure, with each allowed origin followed immediately by a vibronic origin of alternate polarization; assignments for these additional vibronic origins are not explicitly provided in Figure 2, where only two of the four resolved low-energy peaks are labeled. For the Soret bands, only one unresolved peak is observed. Other weak bands are observed at higher energy than the Soret band, and these are known as the N, L, M, etc. bands.

The basic interpretation of the spectrum of porphyrin was put forward originally by Gouterman,[12,13] who interpreted the main features (the B and Q bands) in terms of a four-orbital model. In this model, transitions from the two highest occupied molecular orbitals (the $5b_{1u}$ and $2a_u$ orbitals) into the two lowest unoccupied molecular orbitals (the near-degenerate $4b_{2g}$ and $4b_{3g}$ orbitals, orbitals that are actually degenerate in metalloporphyrins) give rise to the Q and B bands in the following way:

$$Q_x \text{ or } 1^1B_{3u}\text{: } (5b_{1u} \rightarrow 4b_{2g}) + (2a_u \rightarrow 4b_{3g})$$

$$Q_y \text{ or } 1^1B_{2u}\text{: } (5b_{1u} \rightarrow 4b_{3g}) + (2a_u \rightarrow 4b_{2g})$$

$$B_x \text{ or } 2^1B_{3u}\text{: } (5b_{1u} \rightarrow 4b_{2g}) - (2a_u \rightarrow 4b_{3g})$$

$$B_y \text{ or } 2^1B_{2u}\text{: } (5b_{1u} \rightarrow 4b_{3g}) - (2a_u \rightarrow 4b_{2g})$$

In this description, two near-degenerate transitions (in each symmetry) linearly combine to produce a low-energy transition where the transition dipoles destructively interfere (Q band) and a high-energy transition where the transition dipoles constructively interfere (B band). The N and higher energy bands are not included within this basic model. Pictorial representations of the key orbitals involved in these and other important transitions are shown in Figure 3.

It was not until the early 1990s that ab initio calculations could be used to reliably study the electronic spectrum of porphyrin. A CI study by Yamamoto et al.[14] confirmed the assignment given by Gouterman, although it was noted that additional transitions involving the low-lying $4b_{1u}$ orbital are required to correctly describe the B band. A CASPT2 study by Merchán et al.[15] also agreed with the qualitative Gouterman model, establishing the importance of correlating both the σ and π electrons. Several studies (SAC-CI by Nakatsuji and co-workers[16,17] and STEOM-CC by Bartlett and co-workers[18]) suggested an alternative assignment of the spectrum with the observed B band attributed *only* to the 2^1B_{3u} transition while the N band (the shoulder on the high-frequency side of the B band) attributed to the 2^1B_{2u} transition. However, later studies by Bartlett and co-workers,[19] as well as a CASPT2 study by Serrano-Andrés et al.[20] and a time-dependent density-functional (TD-DFT) study by van Gisbergen et al.,[21] confirm the traditional interpretation. This serves to highlight the difficulties which exist with the accurate evaluation of the electronic spectra of porphyrins, in particular with the reproduction of the observed fact that the B band is extremely intense while the near-resonant N band is only weak.

(12) Gouterman, M. *J. Chem. Phys.* **1959**, *30*, 1139.
(13) Gouterman, M. *J. Mol. Spectrosc.* **1961**, *6*, 138.
(14) Yamamoto, Y.; Noro, T.; Ohno, K. *Int. J. Quantum Chem.* **1992**, *42*, 1563.
(15) Merchán, M.; Ortí, E.; Roos, B. O. *Chem. Phys. Lett.* **1994**, *226*, 27.
(16) Nakatsuji, H.; Hasegawa, J.; Hada, M. *J. Chem. Phys.* **1996**, *104*, 2321.
(17) Tokita, Y.; Hasegawa, J.; Nakatsuji, H. *J. Phys. Chem. A* **1998**, *102*, 1843.
(18) Nooijen, M.; Bartlett, R. J. *J. Chem. Phys.* **1997**, *106*, 6441.
(19) Gwaltney, S. R.; Bartlett, R. J. *J. Chem. Phys.* **1998**, *108*, 6790.
(20) Serrano-Andrés, L.; Merchán, M.; Rubio, M.; Roos, B. O. *Chem. Phys. Lett.* **1998**, *295*, 195.
(21) van Gisbergen, S. J. A.; Rosa, A.; Baerends, G. Ricciardi.; Baerends, E. J. *J. Chem. Phys.* **1999**, *111*, 2499.

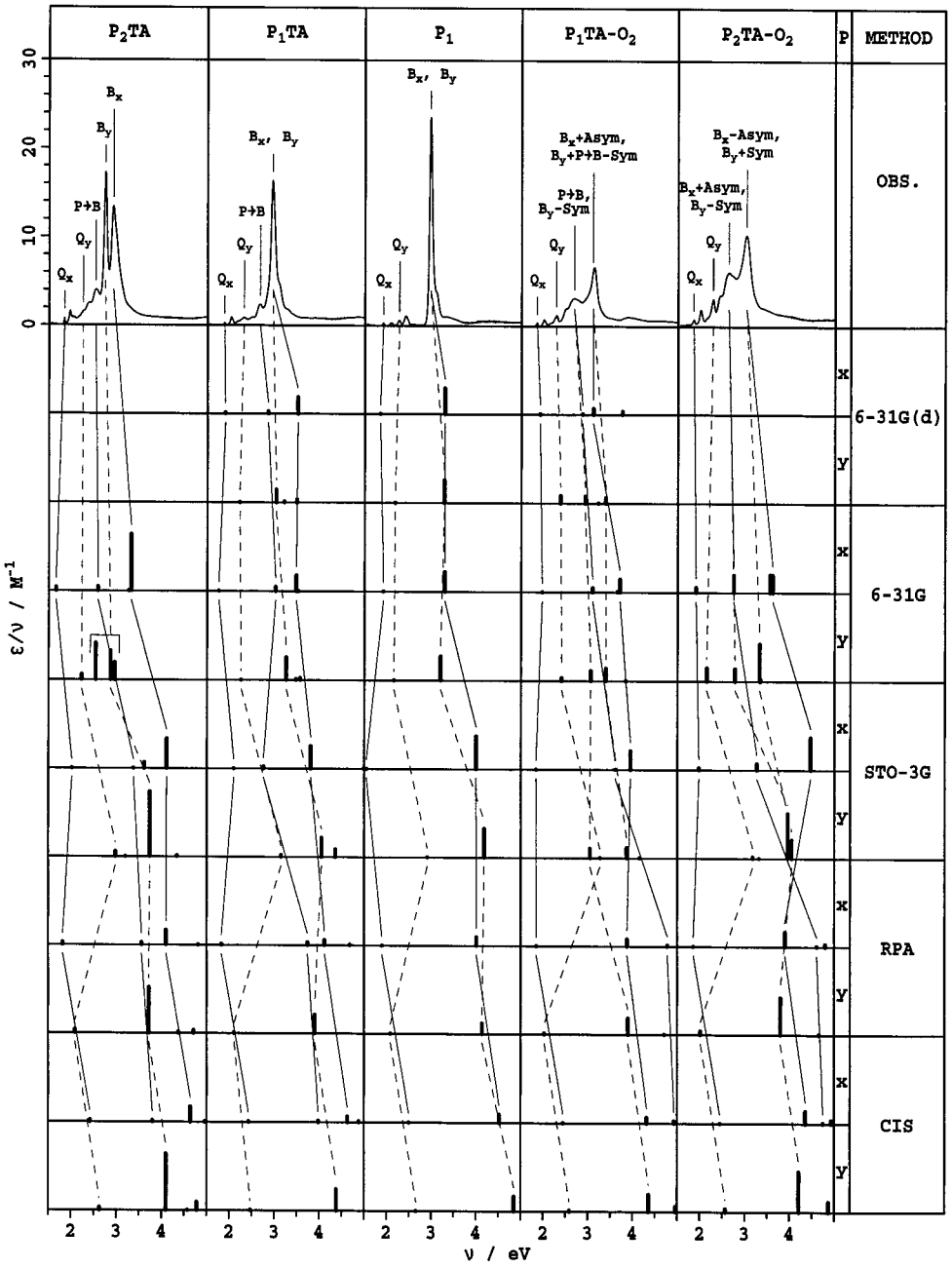

Figure 2. Observed electronic absorption spectra of the oligoporphyrins in light petroleum and their assignments to *x*- or *y*-polarized states in terms of the predictions of CASPT2, CIS, and RPA calculations.

In this paper we describe the electronic absorption spectrum of a homologous series of oligoporphyrins and their constituent molecular fragments, applying CASPT2 to provide assignments. These calculations are supplemented with Tamm−Dancoft configuration interaction singles[22,23] (CIS), random-phase approximation[22] (RPA), and complete neglect of differential overlap[24] (CNDO/S) calculations, and calculated and observed exciton couplings for the TA-bridged dimer are compared. Current density-functional methods have significant problems with extended π systems, e.g., typically predicting that polyacetylene has no band gap. We find that they are useful for geometry optimizations of oligoporphyrins[11] but find them inappropriate for spectroscopic applications.[25]

2. Methods

2.1. Experimental Details. Melting points are uncorrected and were recorded on a Riechert hot stage microscope. Microanalyses were performed by the Microanalytical Unit, School of Chemistry, University of New South Wales. Ultraviolet−visible spectra were recorded on a Hitachi 150-20 spectrophotometer. The abbreviation sh is used to indicate a shoulder on a larger absorbance peak. Infrared spectra were recorded on a Perkin-Elmer model 1600 FT-IR spectrophotometer. Abbreviations used are w, weak; m, medium; s, strong (all for intensity); and br, broad.

(22) Rescigno, C. W. McCurdy Jr.; Rescigno, T. N.; Yeager, D. L.; McKoy, V. In *Methods of electronic structure theory*; Schaefer, H. F., III, Ed.; Plenum: New York, 1977; p 339.
(23) Foresman, J. B.; Head-Gordon, M.; Pople, J. A.; Frisch, M. J. *J. Phys. Chem.* **1992**, *96*, 135.
(24) Del Bene, J.; Jaffe, H. H. *J. Chem. Phys.* **1968**, *48*, 1807, 4050.
(25) Cai, Z.-L.; Sendt, K.; Reimers, J. R. *J. Chem. Phys.*, in press.

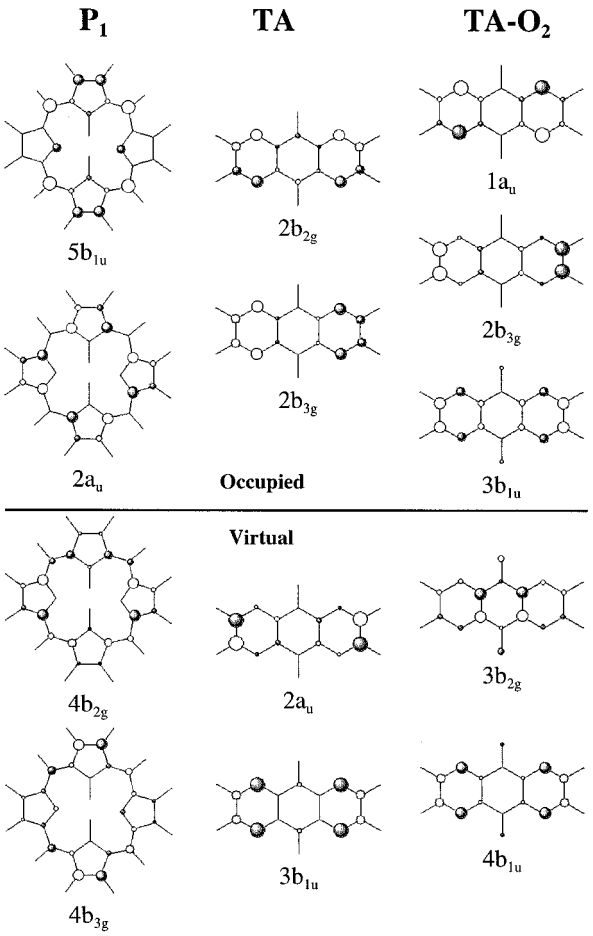

Figure 3. Key molecular orbitals contributing to the observed spectroscopic transitions.

^{1}H NMR spectra were recorded on a Bruker WM-400 (400 MHz) spectrometer. ^{13}C NMR spectra were recorded on a Bruker AC-200F (50 MHz) spectrometer. Tetramethylsilane (TMS) was used as an internal standard. Signals are recorded in terms of chemical shift (δ in parts per million from TMS), number of protons represented (from integration), multiplicity, coupling constants, and assignments, in that order. The following abbreviations for multiplicity are used: s, singlet; d, doublet; t, triplet; ABq, AB quartet; m, multiplet; br, broad. Solvents used were deuterated chloroform ($CDCl_3$) and deuterated dimethyl sulfate (d_6-DMSO).

Electron impact (EI) mass spectra were recorded on an AEI MS902 mass spectrometer. Peaks with a relative intensity of greater than 10% of the base peak are reported. Mass spectra for compounds with molecular weight greater than 1000 amu were recorded by the chemical ionization (CI) technique on a FINNIGAN MAT TSQ mass spectrometer at the Department of Pharmacy, The University of Sydney, by matrix-assisted laser desorption (MALDI) on a VG Instruments MALDI-TOF-SPEC mass spectrometer or on a FINNIGAN LASERMAT mass spectrometer at the Biomedical Mass Spectrometry Unit, University of New South Wales, or by fast atom bombardment (FAB) on a VG Instruments VG ZAB-SEQ FAB+ spectrometer at the Australian National University, Canberra.

Pyridine was distilled and stored over 4 Å molecular sieves or potassium hydroxide. Toluene was distilled and stored over sodium wire. Deoxygenation was achieved by bubbling dry nitrogen through the solvent.

Column chromatography was carried out using the flash chromatography technique on Merck silica gel type 9385.

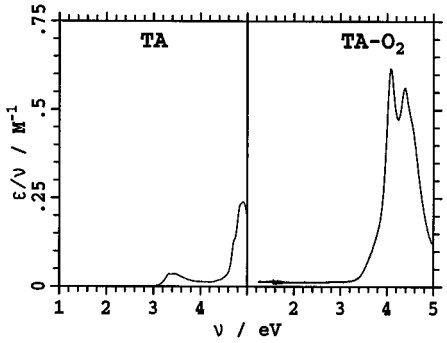

Figure 4. Spectra of TA and TA-O_2 in light petroleum.

2,3,6,7-Tetramethyl-1,4,5,8-tetraazaanthracene (TA). TA was prepared using the method of Armand.[26] MS (MALDI-TOF): *m*/*z* 240 (M + 2, 100). UV−vis (light petroleum): see Figure 4.

2,3,5,6-Tetraamino-1,4-benzoquinone. 2,3,5,6-Tetraamino-1,4-benzoquinone was prepared using the method of Wallenfels and Draber[27] in a yield of 81%, mp > 320 °C (lit.[27] decomposes at 260 °C).

2,3,5,6-Tetraamino-1,4-hydroquinone Tetrahydrochloride. 2,3,5,6-Tetraamino-1,4-hydroquinone tetrahydrochloride was prepared from 2,3,5,6-tetraamino-1,4-benzoquinone using the method of Wallenfels and Draber[27] in a yield of 83%. The recommended method of purification was found to decompose the product, so it was used without purification.

2,3,6,7-Tetramethyl-1,4,5,8-tetraaza-9,10-anthraquinone (TA-O_2). 2,3-Butanedione (757 mg, 8.8 mmol) and 2,3,5,6-tetraamino-1,4-benzoquinone (500 mg, 3.0 mmol) were stirred in a dry, deoxygenated mixture of pyridine (15 mL) and toluene (11 mL) under nitrogen for 4 days. The solution was filtered and the residue repeatedly washed with dichloromethane (including suspending the solid in refluxing dichloromethane for 1−2 h) until filtration gave only a small amount of black residue. The solvent was removed from the combined dichloromethane filtrates to give a yellow powder, which was precipitated from chloroform by concentrating the solution to give TA-O_2 (542 mg, 67%) as a pale yellow powder, mp > 320 °C (lit.[28] decomposes at 326−327 °C). UV−vis ($CHCl_3$): 235 (log ϵ 3.80), 273sh (4.27), 282 (4.33), 303 (4.35) nm. IR ($CHCl_3$): 3683w, 3016m (CH_3), 1701s (C═O), 1601w (C═N), 1546m, 1395m, 1328m, 1224s, 1206s, 965m cm^{-1}. ^{1}H NMR ($CDCl_3$): δ 2.87 (s, CH_3). ^{13}C NMR ($CDCl_3$): δ 23.2 (CH_3), 142.0, 159.9, 180.1 (C═O). MS (EI): *m*/*z* 171 (14), 186 (39), 268 (M^+, 100).

Porphyrin−Tetraazaanthracene P_1TA. A mixture of 2,3-dioxo-5,10,15,20-tetrakis(3,5-di-*tert*-butylphenyl)chlorin (301 mg, 0.275 mmol) and 1,2,4,5-benzenetetramine tetrahydrochloride (95.5 mg, 0.336 mmol), under oxygen-free nitrogen was dissolved in deoxygenated dry pyridine (39 mL). The solution was stirred in the dark under nitrogen for 28 h and then transferred under nitrogen by cannula to a flask containing deoxygenated 2,3-butanedione (0.3 mL). The solution was stirred in the dark under nitrogen for 7 days. Dichloromethane (50 mL) was added, and the organic layer was washed with hydrochloric acid (3 M, 3 • 60 mL), water (60 mL), sodium carbonate solution (5%, 60 mL), and water (60 mL) and then dried over anhydrous sodium sulfate, filtered, and evaporated to dryness. The residue was chromatographed over silica (dichloromethane−light petroleum, 1:1) to yield porphyrin−tetraazaanthracene P_1TA (323 mg, 97%) as a red-brown solid. A sample for analysis, recrystallized from a dichloromethane−methanol mixture, had mp > 350 °C. UV−vis ($CHCl_3$): 253 (log ϵ 4.59), 379sh (4.64), 404sh (4.96), 426 (5.49), 464sh (4.72), 539 (4.28), 612 (4.11), 660 (3.51), 715 (2.70). IR ($CHCl_3$): 3353w (inner NH), 2965s, 2904w, 2868w, 1593m, 1476w, 1423w, 1364w, 1265s, 1100w, 990w, 896w cm^{-1}. ^{1}H NMR ($CDCl_3$): δ −2.37 (2 H, s, inner NH), 1.52 (36 H, s,

(26) Armand, J.; Boulares, L.; Bellec, C.; Pinson, J. *Can. J. Chem.* **1987**, *65*, 1619.
(27) Wallenfels, K.; Draber, W. *Liebigs Ann. Chem.* **1963**, 55.
(28) Yamashita, Y.; Suzuki, T.; Saito, G.; Mukai, T. *Chem. Lett.* **1986**, 715.

Table 1. Active Spaces Used in CASPT2 Calculations[a]

C_{2v}								D_{2h}									
	$P_1TA\ ^1A_1$		$P_1TA\ ^1B_1$		$P_1TA\text{-}O_2$				TA		$TA\text{-}O_2$		P_1		P_2TA	$P_2TA\text{-}O_2$	
	6-31G(d)		6-31G(d)						6-31G(d)		6-31G(d)		6-31G(d)		6-31G		
rep	6-31G (14/13)	STO- 3G (8/10)	6-31G (14/13)	STO-3G (8/9)	6-31G(d) (8/14)	6-31G (14/13)	STO-3G (8/9)	rep	6-31G (8,8)	STO-3G (4/4)	6-31G (8,8)	STO-3G (6/5)	6-31G (12/12)	STO-3G (4/5)	STO-3G (14/14)	6-31G (10/15)	STO-3G (14/15)
b_2	7, 7	9, 5	7, 7	9, 4	10, 7	8, 7	10, 4	b_{1u}	1, 2	2, 1	2, 2	2, 2	2, 4	4, 1	8, 3	8, 5	8, 5
								b_{3g}	1, 2	1, 1	1, 2	1, 1	2, 3	3, 1	7, 3	8, 4	8, 2
a_2	5, 6	6, 5	5, 6	6, 5	6, 7	5, 6	6, 5	a_u	0, 2	1, 1	0, 2	0, 1	1, 2	1, 2	5, 4	5, 3	5, 3
								b_{2g}	1, 2	1, 1	1, 2	2, 1	2, 3	3, 1	4, 4	6, 3	4, 5

[a] Listed as number of orbitals doubly occupied, number of orbitals in the active space of size *n*/*m*, where *n* is the number of electrons distributed in *m* active orbitals.

tert-butyl H), 1.54 (36 H, s, *tert*-butyl H), 2.86 (6 H, s, CH_3), 7.81 (2 H, t, $J = 1.8$ Hz, Ar-H_p), 7.95 (2 H, t, $J = 1.8$ Hz, Ar-H_p), 8.02 (4 H, d, $J = 1.8$ Hz, Ar-H_o), 8.10 (4 H, d, $J = 1.8$ Hz, Ar-H_o), 8.59 (2 H, s, H-9″ and H-10″), 8.77 (2 H, s, β-pyrrolic H-12 and H-13), 8.97 and 9.00 (4 H, ABq, $J = 5.0$ Hz, β-pyrrolic H). MS (MALDI-TOF): *m*/*z* 1245 (M^+, 100). Anal. Calcd for $C_{86}H_{100}N_8$: C, 82.91; H, 8.09; N, 8.99. Found: C, 83.00; H, 8.23; N, 8.72.

Porphyrin−Quinone $P_1TA\text{-}O_2$. 2,3-Dioxo-5,10,15,20-tetrakis(3,5-di-*tert*-butylphenyl)chlorin (85 mg, 0.078 mmol) and 2,3,5,6-tetraamino-1,4-benzoquinone (13 mg, 0.081 mmol) were stirred at reflux in dry, deoxygenated pyridine (10 mL) under nitrogen in the dark for 1 h. 2,3-Butanedione (13 μL, 0.15 mmol) was added and the solution stirred at reflux for a further 4 h. The stirred solution was allowed to cool overnight and worked up by the usual procedure. The product was purified by column chromatography using dichloromethane as the eluent. The desired porphyrin−quinone adduct $P_1TA\text{-}O_2$ (44 mg, 45%) was obtained as a dark brown-black solid, mp > 320 °C (from chloroform/methanol). UV−vis ($CHCl_3$): 252 (log ϵ 4.24), 282 (4.28), 321 (4.38), 407 (5.12), 468sh (4.56), 549 (4.13), 626 (3.74), 681 (3.53) nm. IR ($CHCl_3$): 3352w (inner NH), 2968s, 2955m, 1700s (C═O), 1593m, 1477m, 1364m, 1294m, 1159s cm^{-1}. ^1H NMR ($CDCl_3$): δ −2.44 (2 H, s, inner NH), 1.23 (36 H, s, *tert*-butyl H), 1.48 (36 H, s, *tert*-butyl H), 2.87 (6 H, s, CH_3), 7.79 (2 H, t, $J = 1.6$ Hz, Ar-H_p), 7.94 (2 H, t, $J = 1.6$ Hz, Ar-H_p), 7.98 (4 H, d, $J = 1.6$ Hz, Ar-H_o), 8.06 (4 H, d, $J = 1.6$ Hz, Ar-H_o), 8.77 (2 H, s, β-pyrrolic H-12 and H-13), 8.97 and 9.06 (4 H, ABq, $J = 4.9$ Hz, β-pyrrolic H-7, H-8, H-17, and H-18). MS (FAB): *m*/*z* 1263 (14), 1274 (M^+, 4), 1277 (M + 3, 100). Anal. Calcd for $C_{86}H_{98}N_8O_2 + 0.25CHCl_3$: C, 79.35; H, 7.58; N, 8.58. Found: C, 79.46; H, 7.62; N, 8.25.

Bisporphyrin P_2TA. This compound was prepared by the condensation of 2 equiv of 2,3-dioxo-5,10,15,20-tetrakis(3,5-di-*tert*-butylphenyl)-chlorin and 1,2,4,5-benzenetetramine as is described in the literature.[29]

Quinonoid Bisporphyrin $P_2TA\text{-}O_2$. Method 1. 2,3-Dioxo-5,10,15,20-tetrakis(3,5-di-*tert*-butylphenyl)chlorin (62 mg, 0.057 mmol) and 2,3,5,6-tetraamino-1,4-benzoquinone (6 mg, 0.03 mmol) were stirred at reflux in dry, deoxygenated pyridine (2 mL) under nitrogen for 4 h. The reaction was worked up by the usual procedure, and quinonoid bisporphyrin $P_2TA\text{-}O_2$ (52 mg, 80%) was isolated by column chromatography, with dichloromethane/light petroleum (1:3 and then 2:5) as the eluent, to give the product as a dark brown solid, mp > 320 °C. UV−vis ($CHCl_3$): 315 (log ϵ 4.57), 418 (5.40), 472sh (5.11), 547 (4.61), 621 (4.29), 675 (3.91) nm. IR ($CHCl_3$): 3352w (inner NH), 2966s, 2906w, 2870w, 1701m (C═O), 1593m, 1477m, 1364m, 1164s cm^{-1}. ^1H NMR ($CDCl_3$): δ −2.44 (4 H, s, inner NH), 1.56 (72 H, s, *tert*-butyl H), 1.64 (72 H, s, *tert*-butyl H), 7.82 (4 H, t, $J = 1.8$ Hz, Ar-H_p), 7.98 (4 H, t, $J = 1.2$ Hz, Ar-H_p), 8.04 (8 H, d, $J = 1.2$ Hz, Ar-H_o), 8.09 (8 H, d, $J = 1.8$ Hz, Ar-H_o), 8.79 (4 H, s, β-pyrrolic H-12, H-13, H-12′, and H-13′), 8.98 and 9.02 (8 H, ABq, $J = 4.8$ Hz, β-pyrrolic H). MS (FAB): *m*/*z* 1026 (13), 1065 (22), 1082 (100), 1110 (36), 1152 (13), 2283 (M^+, 12). Anal. Calcd for $C_{158}H_{184}N_{12}O_2$: C, 83.12; H, 8.12; N, 7.36. Found: C, 82.92; H, 8.30; N, 7.12.

Method 2. 2,3-Dioxo-5,10,15,20-tetrakis(3,5-di-*tert*-butylphenyl)-chlorin (48 mg, 0.044 mmol) and 2,3,5,6-tetraamino-1,4-hydroquinone tetrahydrochloride (11 mg, 0.035 mmol) were stirred at reflux in dry, deoxygenated pyridine (2 mL) under nitrogen for 4.75 h. The reaction was worked up by the usual procedure, and the residue chromatographed with dichloromethane/light petroleum (1:4 and then 1:3) as the eluent to give two products. The first rapidly decomposed to quinonoid bisporphyrin $P_2TA\text{-}O_2$ and has been tentatively assigned the structure of hydroquinonoid bisporphyrin (3 mg, 6%). ^1H NMR ($CDCl_3$): δ −2.55 (4 H, s, inner NH), 1.53 (72 H, s, *tert*-butyl H), 1.55 (72 H, s, *tert*-butyl H), 7.82 (4 H, t, coinciding with a signal arising from $P_2TA\text{-}O_2$ present in the sample, Ar-H_p), 7.95 (4 H, t, $J = 1.7$ Hz, Ar-H_p), 8.08 (16 H, br s, coinciding with a signal arising from $P_2TA\text{-}O_2$, Ar-H_o), 8.77 (4 H, s, β-pyrrolic H-12, H-13, H-12′, and H-13′), 8.96−9.00 (8 H, m, overlapping AB quartets arising from $P_2TA\text{-}O_2$ and hydroquinone, β-pyrrolic H), 9.41 (2 H, s, OH).

The second product obtained was quinonoid bisporphyrin $P_2TA\text{-}O_2$ (13 mg, 25%), cochromatographed with and identical by ^1H NMR spectroscopy to an authentic sample.

2.2. Computational Details. All calculations are performed at the optimized B3LYP/3-21G geometries of the molecules.[11] The molecules were placed in the *xy* plane with the pyrrolic hydrogens on the *x*-axis with the long axis parallel to the *y*-axis, as shown in Figure 1. Porphyrin, TA, $TA\text{-}O_2$, P_2TA, and $P_2TA\text{-}O_2$ were constrained to D_{2h} symmetry, while P_1TA and $P_1TA\text{-}O_2$ were constrained to C_{2v} symmetry.

To calculate the electronic spectra of the molecules of interest, second-order multiconfigurational perturbation theory (CASPT2)[30,31] was used. The active spaces of the reference states were chosen to include the orbitals involved in the most important excitations up to 3.5 eV in energy. However, the size of the P_2TA and $P_2TA\text{-}O_2$ molecules prohibited the inclusion of all orbitals of interest in a complete active space SCF (CASSCF)[32,33] calculation. An active space of *n* active electrons in *m* active orbitals is designated (*n*, *m*), and the active spaces used for all molecules are shown in Table 1. Whenever possible, the active space for each basis set is chosen so that a consistent set of orbitals are included for each molecule, facilitating the identification of similar bands in similar molecules. Some trial active spaces resulted in the exclusion of key states and their replacement by low-extinction porphyrin to bridge or similar states. Hence, it is clear that not all transitions in the Soret band region are included in the calculations, but every effort was made to ensure that all significant states are included.

The transition dipole moments were calculated[34,35] at the CASSCF level of theory only. The oscillator strengths were calculated using the CASSCF transition dipole moments and the CASPT2 excitation energies, a combination of methods tested by Roos et al.[36,37] Several

(29) Crossley, M. J.; Burn, P. L. *J. Chem. Soc., Chem. Commun.* **1987**, 39.
(30) Andersson, K.; Malmqvist, P.-Å.; Roos, B. O.; Sadlej, A. J.; Wolinski, K. *J. Chem. Phys.* **1990**, *94*, 5483.
(31) Andersson, K.; Malmqvist, P.-Å.; Roos, B. O. *J. Chem. Phys.* **1992**, *96*, 1282.
(32) Roos, B. O.; Taylor, P. R.; Siegbahn, P. E. S. *Chem. Phys.* **1980**, *48*, 157.
(33) Roos, B. O. In *Ab initio Methods in Quantum Chemistry*; Lawley, K. P., Ed.; Wiley: Chichester, U.K., 1987; p 399.
(34) Malmqvist, P.-Å. *Int. J. Quantum Chem.* **1986**, *30*, 479.
(35) Malmqvist, P.-Å.; Roos, B. O. *Chem. Phys. Lett.* **1989**, *155*, 189.

basis sets were used in this study: the largest of these, 6-31G(d),[38] was not feasible to use for the porphyrin dimers, but 6-31G and STO-3G[39] were used for all molecules. As these basis sets (and the above-mentioned active spaces) are smaller than is usual for CASPT2 calculations, errors in calculated transition energies in excess of the typical 0.2 eV maximum error are anticipated. Also, no corrections for solvation, which would lower relative charge-transfer transition energies, are included in this work.

The CASSCF and CASPT2 calculations were performed using the MOLCAS 4.1 program.[40] The modified Fock operator G3[41] was used throughout, as recommended by Andersson, to remove a systematic error in the standard CASPT2 method. A level shift to the Hamiltonian operator was also applied to remove intruder states: 0.4 au was used for porphyrin (as recommended by Serrano-Andrés et al.[20]), TA, and P_1TA, while a shift of 0.5 au was found necessary for $P_1TA\text{-}O_2$ and $P_2TA\text{-}O_2$ and 0.6 au for $TA\text{-}O_2$.

In addition, CIS and RPA calculations are performed using TURBOMOLE[42] using the 3-21G basis set, while the CNDO/S calculations are performed using our own INDO-MRCI program.[43] These methods are of lower accuracy than CASPT2 but treat all excitations on an equal footing; they serve to verify our conclusion that all important states are included in the CASPT2 calculations and provide estimates of the exciton couplings without nonsystematic variations.

3. Molecular Architecture

Porphyrin−tetraazaanthracene P_1-TA was prepared in 97% yield by first stirring porphyrindione $P_1\text{-}O_2$ with 1.2 equiv of 1,2,4,5-benzenetetraamine tetrahydrochloride in pyridine under nitrogen in the dark for 28 h to give the diamine intermediate. The pyridine solution of the intermediate was combined with 2,3-butanedione and stirred under nitrogen, in the dark, for 7 days (Scheme 1).

2,3,5,6-Tetraamino-1,4-benzoquinone was prepared from chloranil in two steps by the method of Wallenfels and Draber.[27] Chloranil was reacted with potassium phthalimide to give 2,3,5,6-tetraphthalimido-1,4-benzoquinone, which was treated with hydrazine hydrate to give the corresponding tetraaminobenzoquinone.

The symmetrical quinonoid bisporphyrin $P_2TA\text{-}O_2$ was prepared by stirring porphyrindione $P_1\text{-}O_2$ with 2,3,5,6-tetraamino-1,4-benzoquinone in pyridine with heating for 4 h (Scheme 2). Yields of up to 80% of the quinonoid bisporphyrin $P_2TA\text{-}O_2$ have been achieved, although more typically 30−40% yields of the desired product were obtained. These poor yields have been attributed to the purity of the tetraaminobenzoquinone because there was little variation in other factors such as temperature, reaction time, and concentration.

Scheme 1 [a]

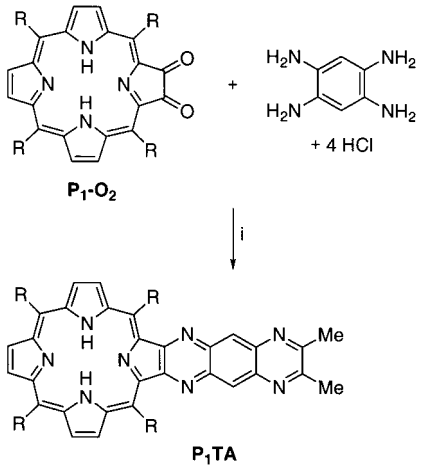

[a] Reagents and conditions: (i) pyridine, N_2, heat, 1 h, then 2,3-butanedione in pyridine, stir, 7 d, R = 3,5-$Bu^t_2C_6H_3$.

Scheme 2 [a]

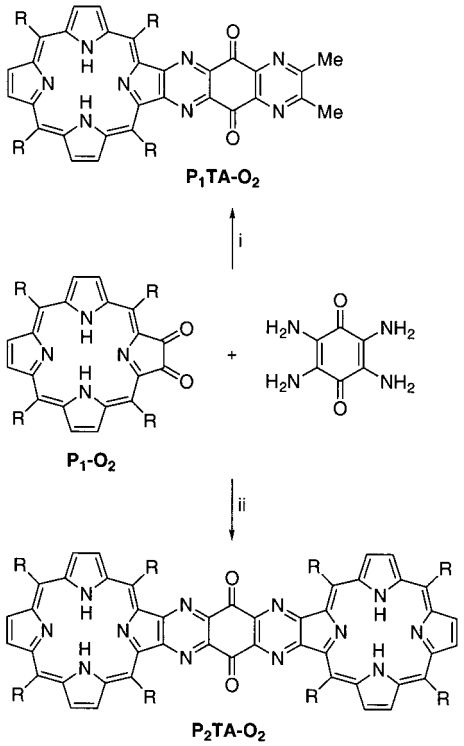

[a] Reagents and conditions: (i) pyridine, N_2, heat, 1 h, then 2,3-butanedione in pyridine, heat, 4 h, R = 3,5-$Bu^t_2C_6H_3$; (ii) pyridine, N_2, heat, 4 h, R = 3,5-$Bu^t_2C_6H_3$.

The structure of the quinonoid bisporphyrin $P_2TA\text{-}O_2$ was confirmed spectroscopically and by microanalysis. In particular, the ^{1}H NMR spectrum showed the D_{2h} symmetry of the molecules. The β-pyrrolic protons (H-12, H-13, H-12′, and H-13′) at the ends of the long axis of symmetry are all equivalent and gave rise to a four-proton singlet. The remaining β-pyrrolic protons gave rise to a single AB quartet as all eight protons are in only two different environments.

The bridging units lacking the porphyrin end groups and having methyl groups instead ($TA\text{-}O_2$ and TA) were similarly prepared by condensation of tetramines with 2,3-butanedione (Scheme 3).

(36) Roos, B. O.; Fülscher, M. P.; Malmqvist, P.-Å.; Merchán, M.; Serrano-Andrés, L. In *Quantum Mechanical Electronic Structure Calculations with Chemical Accuracy*; Langhoff, S. R., Ed.; Kluwer Academic: Dordrecht, The Netherlands, 1995; p 357.
(37) Roos, B. O.; Andersson, K.; Fülscher, M. P.; Malmqvist, P.-Å.; Serrano-Andrés, L.; Pierloot, K.; Merchán, M. In *Advances in Chemical Physics: New Methods in Quantum Mechanics, vol. XCIII*; Prigogine, I., Rice, S. A., Eds.; John Wiley: New York, 1996; p 219.
(38) Hariharan, P. C.; Pople, J. A. *Theor. Chim. Acta* **1973**, *28*, 213.
(39) Hehre, W. J.; Stewart, R. F.; Pople, J. A. *J. Chem. Phys.* **1969**, *51*, 2657.
(40) Andersson, K.; Blomberg, M. R. A.; Fülscher, M. P.; Karlström, G.; Lindh, R.; Malmqvist, P.-Å.; Neogrády, P.; Olsen, J.; Roos, B. O.; Sadlej, A. J.; Seijo, L.; Serrano-Andrés, L.; Siegbahn, P. E. M.; Widmark, P.-O. *Molcas Version 4*; University of Lund: Lund, 1997.
(41) Andersson, K. *Theor. Chim. Acta* **1995**, *91*, 31.
(42) Ahlrichs, R.; Bär, M.; Baron, H.-P.; Bauernschmitt, R.; Böcker, S.; Ehrig, M.; Eichkorn, K.; Elliot, S.; Haase, F.; Häser, M.; Horn, H.; Huber, C.; Huniar, U.; Kattannek, M.; Kölmel, C.; Kollwitz, M.; Ochsenfeld, C.; Öhm, H.; Schäfer, A.; Schneider, U.; Treutler, O.; von Arnim, M.; Weigend, F.; Weis, P.; Weiss, H. *TURBOMOLE*; Quantum Chemistry Group, University of Karlsruhe: Karlsruhe, Germany, 1997; Version 4.
(43) Zeng, J.; Hush, N. S.; Reimers, J. R. *J. Phys. Chem.* **1995**, *99*, 10459.

Table 2. Electronic Transition Energies ΔE, eV, and Oscillator Strengths f in Free-Base Porphyrin and P_1

		obsd			CASP2 (this work)			CASPT2[e]		TD-DFT[f]		SAC-CI[g]		EOM-CCSD[h]	
state	assign.	ΔE	ΔE[c]	f[d]	6-31G(d)	6-31G	f[i]	ΔE	f	ΔE	f	ΔE	f	ΔE	f
1^1B_{3u}	Q_x	1.98−2.02[a]	1.91	0.01	1.85	1.92	2×10^5	1.63	0.004	2.16	0.01	1.77	0.0028	1.75	0.0007
2^1B_{3u}	B_x	3.13−3.33[b]	∼2.97	1.15	3.29	3.29	1.4	3.12	0.704	2.98	0.1338	3.47	0.772	3.47	0.693
3^1B_{3u}	N_x	3.65[d]	∼3.4	<0.1	3.64	3.45	0.34	3.53	0.833	3.47	0.7293	4.20	1.32	4.06	0.931
1^1B_{2u}	Q_y	2.33−2.42a[a]	2.27	0.06	2.18	2.16	0.17	2.11	0.002	2.29	0.0005	2.01	0.0132	2.40	0.013
2^1B_{2u}	B_y	3.13−3.33[b]	∼2.97	1.15	3.28	3.20	1.20	3.08	0.911	2.98	0.04	3.73	1.62	3.62	1.20
3^1B_{2u}	N_y	3.65[d]	∼3.4	<0.1	3.81	3.77	0.20	3.42	0.458	3.41	0.8962	5.15	0.339	4.35	0.422
2^1A_g	sym				3.61	3.78	0					4.24	0		
3^1A_g	sym				3.64	3.84	0					4.74	0		
4^1A_g	sym				3.76	3.96	0					5.28	0		
1^1B_{1g}	asym				2.97	3.12	0					3.45	0		
2^1B_{1g}	asym				3.24	3.25	0					5.44	0		
3^1B_{1g}	asym				3.76	3.98	0					5.80	0		

[a] References 44, 50, and 51. [b] References 44, 51, and 52. [c] This work, tetra-*meso*-substituted porphyrin. [d] Reference 44. [e] Reference 15. [f] Reference 21. [g] References 16 and 17. [h] Reference 18. [i] CASSCF/6-31G(d).

Scheme 3 [a]

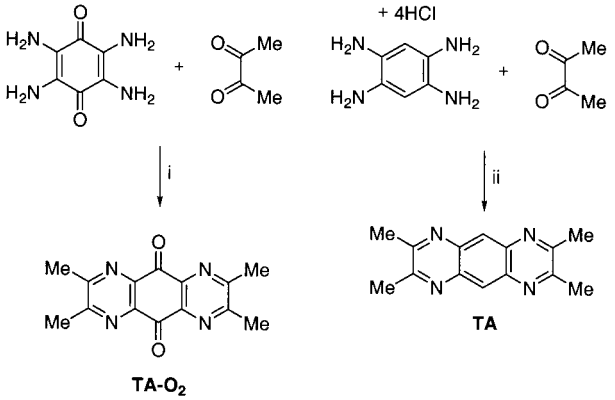

[a] Reagents and conditions: (i) pyridine−toluene, N_2, stir, 4 d; (ii) pyridine−toluene, N_2, stir, 4 d, filter, suspend solid in refluxing dichloromethane 1−2 h.

4. Molecular Spectroscopy

Figures 2 and 4 show the observed spectra, depicting ϵ/ν as a function of $h\nu$, where ν is the frequency and ϵ is the molar extinction. In this representation, the areas of the spectral bands correspond simply to the square of the transition moment of the band. Lines representing the calculated vertical excitation energies whose heights are proportional to the calculated f/ν, where f is the oscillator strength, and the suggested assignments are also shown. The nature of the calculated transitions is obtained by examination of the dominant configurations in the transition; key orbitals are sketched in Figure 3. This procedure is not necessarily straightforward to apply, however, due to rotations of the molecular orbitals, and the nature of what appears to be the same band can change somewhat with the basis set. Numerically, all of the data shown in these figures are tabulated in Tables 2−8, one table for each molecule. Unless otherwise specified, all computational methods gave rise to the same qualitative interpretation of the observed spectra. The CASPT2 results include both allowed and forbidden (π, π^*) transitions, but no calculations of (n, π^*) transitions are presented; a proper assignment of the spectra of TA and TA-O_2 is not attempted as this would require their inclusion. Note also that the transitions calculated using CASPT2 correspond to the lowest-energy ones of each particular symmetry but no information is available concerning transitions of higher energy. Such transitions do occur within the observed frequency range, and our CIS and RPA calculations provide information concerning them; they are not believed to contribute significantly to the spectroscopy. We consider the results obtained for each molecule in turn.

4.1. P_1. The calculated electronic spectrum of porphyrin is shown in Table 2, along with previous theoretical and experimental results. While the assignment of the experimental spectrum of porphyrin (in particular the higher energy B, N, etc. bands) has been controversial, two recent works[20,21] conclude that the traditional interpretation of a series of pairs ($^1B_{2u}$ and $^1B_{3u}$, respectively) of excitations are responsible for the observed bands. Our most extensive calculations, with the large active space and the 6-31G(d) basis set, are in agreement with this interpretation. They depict qualitatively similar results for the Q, B, and N bands to the larger CASPT2 results of Serrano-Andrés et al.,[20] in terms of both the excitation energies and the important configurations contributing to the excited-state wave functions. The two lowest-energy transitions (Q_x and Q_y) are well described by the Gouterman model.[12,13] The next two transitions (contributing to the intense (Soret) B band) are found to have important configurations in their wave functions (in particular involving the $4b_{1u}$ orbital and to a lesser extent $3b_{1u}$) that are not included in the simple Gouterman model.

As the aim of this work is to understand the electronic spectra of porphyrin−bridge and bisporphyrin systems, the porphyrin molecule itself was not studied in such detail as the earlier study by Serrano-Andrés et al.[20] Differences found between the 6-31G(d) results and the 6-31G ones are similar to those found between these and the experimental spectra, with transition energies in error by 0.1−0.2 eV. The Q bands are slightly underestimated in energy, while the B and N bands are slightly overestimated. As a consequence, the Q_x–B_x and Q_y–B_y splittings are calculated to be too large by 0.2−0.3 eV. However, the observed and calculated B to N splittings are in good agreement, but the calculated intensity of the N bands is too large. The details of the B−N mixing and subsequent intensity transfer are very sensitive to the accuracy of the computational method.[44] All of the experimental data reported herein are for tetra-*meso*-substituted porphyrins, except for Table 2 in which the corresponding results for free-base porphyrin are also provided to show that the effects of this substitution are to induce small red shifts on the order of 0.1−0.2 eV. These shifts are on the

(44) Edwards, L.; Dolphin, D. H.; Gouterman, M.; Adler, A. D. *J. Mol. Spectrosc.* **1971**, *38*, 16.

Table 3. Electronic Transition Energies ΔE, eV, and Oscillator Strengths f in TA

		obsd	CASPT2		
state	pol	ΔE	6-31G(d)	6-31G	f [a]
1^1B_{3u}	x	3.4	3.19	3.56	0.15
1^1B_{2u}	y	2.8[b]	3.02	3.17	0.08
2^1A_g			5.72	5.91	0
1^1B_{1g}			4.00	4.31	0

[a] CASSCF/6-31G(d) values. [b] Assignment of the observed band is uncertain; various non-(n, π^*) possibilities are indicated.

same order as the errors in the band positions evaluated using the 6-31G(d).

Porphyrin has additional forbidden $\pi \rightarrow \pi^*$ transitions of $^1B_{1g}$ and ^1A_g symmetry that are not included in the Gouterman four-orbital model. In molecules such as P_1TA and P_1TA-O_2 the presence of the bridge molecule reduces the molecular symmetry to C_{2v}, causing the $^1B_{1g}$ and ^1A_g transitions to have $^1B_1$ and $^1A_1$ symmetry, respectively, hence becoming weakly allowed. Such transitions may also appear in the dimers as, for these, the local symmetry for each individual porphyrin remains C_{2v}. Hence, a study of these optically inactive porphyrin transitions was undertaken; their properties have been investigated in previous SAC-CI studies[16,17] only. In all, six excited states were located in the energy range of interest; see Table 2. Using the 6-31G-(d) basis, the lowest $^1B_{1g}$ state was predicted to be lower in energy than the Soret band, while the next $^1B_{1g}$ state was of comparable energy. For each of these six states, the wave function involved both single and double excitation. For example, the lowest ^1A_g state contains not only transitions such as b_{2g} to b_{2g} involving orbitals from outside the four-orbital model but also double excitations of the Q_x type. To correctly represent both these transitions and the N bands, eight orbitals must be included in the active space, as detailed in Table 1.

4.2. TA. The observed absorption spectrum of TA in light petroleum is shown in Figure 4 and summarized in Table 3, along with the computed spectra. Experimentally, a relatively weak band with discernible vibrational structure is found centered at 4.8 eV, a weaker band centered at 3.4 eV, and an extremely weak shoulder centered at ca. 2.8 eV. The 6-31G(d) calculations locate an x-polarized transition near the one observed at 3.4 eV involving the two orbitals shown in Figure 3, and predict a very weak y-polarized one at slightly lower energy which could account for the shoulder. Alternatively, (n, π^*) transitions not considered could account for the shoulder. Note that, to describe similar transitions that might occur in P_1TA and P_2TA, orbitals corresponding to the TA $3b_{1u}$, $2b_{2g}$, $2b_{3g}$, and $2a_u$ orbitals (see Figure 3) were included in the active space of P_1TA and P_2TA. The features in the observed spectrum of TA are, however, 1−2 orders of magnitude weaker than the features observed in the spectra of the oligoporphyrins.

4.3. TA-O_2. The observed absorption spectrum of TA-O_2 in light petroleum is shown in Figure 4 and summarized in Table 4, along with the computed spectra. Experimentally, the spectrum is dominated by a medium-strength absorption centered at ca. 4.2 eV which is broad and contains resolved vibrational structure; a shoulder at ca. 3.6 eV is also identified. The 6-31G(d) calculations predict a weak y-polarized absorption at 4.6 eV which is assigned to the major band, while the shoulder could be accounted for by either a forbidden (π, π^*) absorption calculated at 4.4 eV or some possible (n, π^*) transition. All

Table 4. Electronic Transition Energies ΔE, eV, and Oscillator Strengths f in TA-O_2

		obsd	CASPT2		
state	pol	ΔE	6-31G(d)	6-31G	f [a]
1^1B_{3u}	x		5.02	5.34	0.40
1^1B_{2u}	y	4.2	4.58	4.83	0.08
2^1A_g			5.09	5.42	0
1^1B_{1g}			4.37	4.78	0

[a] CASSCF/6-31G(d) values.

Table 5. Electronic Transition Energies ΔE, eV, and Oscillator Strengths f in P_1TA

		obsd	CASPT2		
state	assign.	ΔE	6-31G(d)	6-31G	f [a]
1^1B_1	Q_x	1.88	1.90	1.76	0.038
2^1B_1	P → B	2.67	2.85	3.48	0.12
3^1B_1	B_x	2.95	3.51	3.02	0.96
4^1B_1	asym		3.52	3.53	0.0003
2^1A_1	Q_y	2.31	2.22	2.26	0.014
3^1A_1	B_y	2.95	3.03	3.26	0.64
4^1A_1	sym + P → B		3.21	3.48	0.07
5^1A_1	sym		3.49	3.57	0.18

[a] CASSCF/6-31G(d) values.

calculations indicate that the quinonoid system has its strong absorption at much lower energy than does the benzenoid one, in agreement with the observed spectrum and general expectations.[11] The transition responsible for the y-polarized absorption in TA-O_2, however, involves extensive outer-ring character involving all of the orbitals shown in Figure 3. Hence, this transition is distinctly different in nature from the seemingly analogous transition[11] in quinone itself.

The 1^1A_g and 1^1B_{1g} transitions, although forbidden in TA-O_2 due to symmetry, are allowed in P_1TA-O_2 and hence are relevant to this study. However, the 6-31G(d)-calculated transition energies of 5.1 and 4.4 eV, respectively, are considerably higher in energy than those for the porphyrin Soret band. To describe in P_1TA-O_2 and P_2TA-O_2 transitions similar to those described above, the orbitals corresponding to the TA-O_2 $3b_{1u}$, $4b_{1u}$, $2b_{2g}$, $3b_{1g}$, $2b_{3g}$, $3b_{3g}$, and $1a_u$ orbitals (see Figure 3) were identified as important to include in the active spaces of P_1-TA-O_2 and P_2TA-O_2. As for TA, the features in the observed spectrum are much weaker than the features observed in the spectra of the oligoporphyrins.

4.4. P_1TA. The observed absorption spectrum of P_1TA in light petroleum is shown in Figure 2 and summarized in Table 5, along with the computed spectra. Experimentally, the spectrum of this porphyrin plus bridge compound is very similar to that of porphyrin itself, the major differences being an increase in line width and the appearance of a new sharp but weak band at 2.67 eV between the porphyrin Q and B bands. The qualitative conclusion that the fusion of the bridge to the porphyrin provides only minor perturbations to the respective electronic structures is supported by the molecular orbital calculations: the porphyrin orbitals change only slightly, with the wave functions of the key orbitals becoming concentrated close to the bridge moiety, and the key bridge orbitals also change only slightly, becoming concentrated toward the center of the TA moiety.

The assignment of the Q and B bands in P_1TA is quite straightforward, although the B_x and B_y transitions are predicted using the 6-31G(d) basis to split apart by 0.5 eV, an effect which

Table 6. Electronic Transition Energies ΔE, eV, and Oscillator Strengths f in P_2TA

		obsd	CASPT2	
state	assign.	ΔE	6-31G	f [a]
1^1B_{3u}	Q_x	1.84	1.66	0.096
2^1B_{3u}	P → B	2.53	2.59	0.17
3^1B_{3u}	asym		3.27	0.048
4^1B_{3u}	B_x	2.92	3.32	3.05
1^1B_{2u}	Q_y	2.25	2.23	0.19
2^1B_{2u}	P → B		2.54[b]	1.51
3^1B_{2u}	B_y	2.74	2.87[b]	1.34
$41B_{2u}$	B → B + B_y		2.96	0.81
1^1B_{1g}	Q_x		1.67	0
2^1B_{1g}	asym		3.26	0
3^1B_{1g}	B_x + N_x + asym		3.15[b]	0
4^1B_{1g}	B_x		3.52[b]	0
2^1A_g	Q_y		2.29	0
3^1A_g	tripsinglet		2.87	0
4^1A_g	B_y		3.32	0
5^1A_g	sym		3.95	0

[a] CASSCF/6-31G values. [b] Pairs are strongly mixed.

is not observed. Similar frequency changes are also calculated for the Q bands; these may arise from the discontinuous variations in the CASSCF active space which necessarily accompany calculations of this type on different molecules, and are indicative of the inherent errors in the computed results. A significant feature of the new band at 2.67 eV is its apparently sharp profile, suggesting that it does not contain substantial bridge character. It is assigned to 3^1B_1, an *x*-polarized state of essentially porphyrin to bridge (P → B) charge-transfer character, mixed slightly with B_x. For this excitation, the most important bridge orbital appears to be $3b_{1u}$, but the TA orbitals are quite strongly mixed.

4.5. P_2TA. The observed absorption spectrum of P_2TA in light petroleum is shown in Figure 2 and summarized in Table 6, along with computed spectra obtained using the smaller basis sets only. Unfortunately, it was not possible to include all the desired active orbitals in the active space (see earlier), and effectively the active orbitals were chosen on the basis of their SCF energy. Among others, the four Gouterman orbitals for each porphyrin fragment as well as the four bridge orbitals identified in the discussion concerning TA are included; see Figure 3.

Experimentally, the B transition is observed to split into two, with one component found at the same frequency as in P_1TA while the other is red shifted by ca. 0.2 eV. For the B_x band, the 6-31G calculations predict that on dimer formation B_x is blue shifted by 0.19 eV while B_y is red shifted; however, B_y is placed in resonance with the P → B transitions, which has been significantly red-shifted from its frequency in P_1TA. This resonance is not a robust feature of the calculations, with the P → B transition remaining at high energy according to CASPT2/STO-3G, RPA/3-21G, and CIS/3-21G. We thus conclude that the lower observed band (maximum at 2.74 eV) is B_y while the upper band (maximum at 2.92 eV) is B_x. The P → B band in the spectrum of P_1TA at 2.67 eV is found in the dimer also, shifted slightly to 2.53 eV. Experimental polarization studies in these films[45] indicate that the higher-energy component is dominantly *x*-polarized, but estimates as to the level of possible *y*-polarized contamination, or estimates of the nature of the 2.67 eV band, are not available.

An interesting feature of the calculations for P_2TA is a prediction of a low-energy totally symmetric band at 2.87 eV.

Table 7. Electronic Transition Energies ΔE, eV, and Oscillator Strengths f in P_1TA-O_2

		obsd	CASPT2		
state	assign.	ΔE	6-31G(d)	6-31G	f [a]
1^1B_1	Q_x	1.85	1.92	1.97	0.036
2^1B_1	B_x	2.68	3.11	3.71	0.32
3^1B_1	P → B	3.10	2.87	3.10	0.04
4^1B_1	asym		3.76	3.65	0.21
1^1A_1	Q_y	2.28	2.38	2.41	0.30
2^1A_1	B_y + sym	2.68	2.93	3.06	0.36
4^1A_1	sym + P → B		3.22	4.15	0.02
3^1A_1	B_y sym + P → B	3.10	3.39	3.40	0.32

[a] CASSCF/6-31G(d) values.

This is a two-electron excitation which arises as the singlet-coupled combination of the ^3Q_y excitations on each porphyrin and is designated a *tripsinglet* band. Its energy is approximately twice that calculated at the same level of theory for the ^3Q_y excitation of the porphyrin monomer, 1.5 eV. It is a robust feature of the spectrum of the dimer and is apparent in the CASPT2/STO-3G, RPA, and CIS calculations of both P_2TA and P_2TA-O_2. A corresponding ^3Q_x band is not readily apparent as for this the calculated monomer energy is much higher, 2.1 eV. Double-excitation bands of this nature have been observed in low-symmetry porphyrin dimers such as the photosynthetic reaction center.[46] For P_2TA-O_2, the tripsinglet band appears at 3.67 eV, and hence this band is clearly sensitive to the environment.

4.6. P_1TA-O_2. The observed absorption spectrum of P_1TA-O_2 in light petroleum is shown in Figure 2 and summarized in Table 7, along with the computed spectra. Experimentally, the Q band region of the spectrum is quite similar to that for porphyrin, but the band at 3.10 eV, in the region of the B bands, is much broader and significantly reduced in intensity while a new, intense and very broad band is observed centered at ca. 2.68 eV. The CASPT2 calculations, as well as the CIS and RPA ones, reproduce the essential qualitative features of the spectrum. However, the methods differ in their interpretation of the spectra, the CASPT2 results indicating that both the 2.68 and 3.10 eV bands contain *x*- and *y*-polarized components arising from resonances between the two B_x transitions and two P → B transitions, while RPA and CIS indicate that the lower band is B_y while the upper band is B_x. These assignments are somewhat compatible, however, as the CASPT2 calculations clearly indicate that the *y*-polarized intensity is red shifted to a much larger extent than is the *x*-polarized component. The large observed widths are more readily understood from the CASPT2 prediction of four rather than two participating electronic states, while polarized spectra in stretched films[45] indicate that the lower frequency component has the greater proportion of *y* polarization.

Little remnant of the quinone transition found in TA-O_2 can be seen in either the observed or calculated spectra. In fact, although the active space chosen was large enough to include many of the TA-O_2 bridge orbitals identified earlier, all but two of these actually rotated out of the active space and the occupation numbers for the remnant orbitals in the subsequent CASPT2 calculations were quite low. The P → B transitions

(45) Azumi, R.; Mutsuyoshi, M.; Kuroda, S.; King, L. G.; Crossley, M. J. *Langmuir* **1995**, *11*, 4056.
(46) Scherer, P. O. J.; Fischer, S. F. *Chem. Phys. Lett.* **1997**, *268*, 133.

Table 8. Electronic Transition Energies ΔE, eV, and Oscillator Strengths f in P_2TA-O_2

		obsd	CASPT2	
state	assign.	ΔE	6-31G	f [a]
1^1B_{3u}	Q_x	1.85	1.91	0.169
2^1B_{3u}	B_x + asym	2.63	2.75	0.79
3^1B_{3u}	asym		3.56	0.0
4^1B_{3u}	B_x − asym	3.03	3.62	1.041
1^1B_{2u}	Q_y	2.28	2.15	0.48
2^1B_{2u}	B_y − sym	2.63	2.78	0.57
3^1B_{2u}	B_y + sym	3.03	3.33	2.03
4^1B_{2u}	sym		3.35	0.13
2^1A_g	Q_y		2.42	0
4^1A_g	B_y		3.54	0
5^1A_g	sym		3.59	0
3^1A_g	tripsinglet		3.67	0
1^1B_{1g}	Q_x		1.94	0
2^1B_{1g}	B_x + P → B		2.84	0
3^1B_{1g}	B_x − P → B		3.54	0
4^1B_{1g}	asym		3.57	0

[a] CASSCF/6-31G values.

involved in the mixing with the B_x and B_y states involve the $4b_{1u}$ orbital on TA-O_2; see Figure 3.

4.7. P_2TA-O_2. The observed absorption spectrum of P_2TA-O_2 in light petroleum is shown in Figure 2 and summarized in Table 8, along with the computed spectra obtained using the smaller basis sets. Experimentally, the spectrum is very similar to that of P_1TA-O_2, the only discernible qualitative difference being a doubling of the extinction due to the presence of two porphyrins per molecule. These results are indicative of minimal inter-porphyrin coupling. While the CASPT2-calculated spectra show much greater variation than do the experimental ones, key features of the assignment such as the contribution from both *x*- and *y*-polarized excitations to both the 2.63 and 3.03 eV absorptions remain. However, while for P_1TA-O_2 the Soret band splitting is attributed to interactions with porphyrin to bridge transitions, here we find interactions with the porphyrin asymmetric transitions instead. Other active spaces were investigated which indicated porphyrin to bridge involvement, but unfortunately no single active space could be found which included all of the desired orbitals. It is hence most likely that CASPT2 predicts involvement of both types of transitions for both molecules, and the large spectral bandwidths also suggest significant bridge involvement in these transitions. The CIS- and RPA-calculated spectra for the two molecules are very similar, however, and while they show typically much larger errors than CASPT2, they are not subject to active-space anomalies.

5. Exciton Coupling

The splitting of the two B bands found for P_2TA is indicative of significant inter-porphyrin coupling within the molecule, but the magnitude of the splitting requires careful interpretation. In the exciton-coupling model for the spectrum, each porphyrin ring is considered to have its own localized electronic transitions. Due to the inter-ring interactions, two linear combinations of each of these transitions form and split apart in energy, one of which is symmetry allowed and visible while the other is symmetry forbidden and not discernible in the spectrum. The two bands seen in the spectrum thus correspond to the allowed components of the coupled B_x and B_y states. If the exciton coupling J is the same for the two sets of states, then the allowed components will each be shifted by the same amount and no energy difference will be observed. Hence, the observed splitting corresponds to the *difference* in the exciton coupling of the B_x and B_y states; for P_2TA this difference, taken as the difference in energy between the peak maxima, is 0.18 eV, while no discernible difference is apparent for P_2TA-O_2.

More details concerning the exciton coupling are provided by the electronic structure calculations, but the simple interpretation of the results in terms of exciton coupling requires the introduction of an effective two-level model[1,7,47] in which only equivalent pairs of localized transitions interact. In reality, all excitations interact, and sometimes the mixing is profound; nevertheless, this method requires that, for each of the allowed Q and B bands, a corresponding forbidden band be found. However, when it is clear that the state of interest is predicted to be in strong resonance with another state, the average state energy is used to estimate the exciton splitting. Symmetry aids this process as the partner for a B_{3u} state must be B_{1g} while one for B_{2u} must be A_g. Paired states are indicated by the assignments shown in Tables 6 and 8. The difference in energy of the members of the pairs is equal to $2|J|$, and the sign of the coupling is determined by noting that if $J > 0$, then the forbidden (antisymmetric linear combination) band will have lower energy than the allowed one.

Exciton couplings obtained using the above procedure, applied to CASPT2/6-31G, CIS/3-21G, RPA/3-21G, and CNDO/S energies, are shown in Table 9, along with the difference in the coupling for the Q_x, Q_y and B_x, B_y pairs and that observed for P_2TA and P_2TA-O_2. These observed couplings are obtained using the assumption that only they control the changes in the spectra observed in going from the bridge + monomer species to the bridged dimer. All observed and calculated splittings for the Q bands are quite small, perhaps with the exception of the moderate −0.13 eV coupling predicted by CASPT2 for P_2TA-O_2. For the Soret bands, the observed and calculated exciton couplings are large only for the B_y band of P_2TA. Quantitatively, the difference in the B_x and B_y couplings as observed is 0.18 eV for P_2TA and ∼0.0 eV for P_2TA-O_2, while the calculated couplings are within the ranges 0.24−0.39 and 0.05−0.11 eV, respectively. Hence, good semiquantitative agreement is found between the observed and calculated exciton couplings. This is very encouraging as the calculated couplings are somewhat uncertain due to the presence of resonances and, for CASPT2, nonsystematic variations associated with the choice of active space, while the experimental couplings are difficult to extract as they require first an authoritative band assignment.

6. Conclusions

The observed Soret bands for the benzenoid species P_1TA and P_2TA are distinctly different, while those for the quinonoid species P_1TA-O_2 and P_2TA-O_2 are very similar. We interpret this on the basis of band assignments in terms of the presence of significant exciton coupling in the benzenoid dimer and minimal coupling in the quinonoid one. These band assignments are based on the results of CASPT2 calculations, supported by a polarization study of P_2TA; they also allow quantitative estimates of the coupling to be deduced from the experimental data, estimates found to be in semiquantitative agreement with CASPT2-, CIS-, RPA-, and CNDO/S-computed values.

(47) Reimers, J. R.; Hush, N. S. *J. Phys. Chem. A* **1999**, *103*, 3066.

Table 9. Calculated and Observed Exciton Couplings *J*, eV[a]

	P_2TA					$P_2TA\text{-}O_2$				
band	obsd[b]	CASPT2 6-31G	CIS 3-21G	RPA 3-21G	CNDO/S	obsd[b]	CASPT2 6-31G	CIS 3-21G	RPA 3-21G	CNDO/S
Q_x	−0.04	−0.01	−0.01	−0.01	0.00	0	−0.02	0.00	0.00	0.00
Q_y	−0.06	−0.03	−0.02	−0.02	0.01	0	−0.13	0.01	−0.01	0.01
Q_x-Q_y	0.02	0.02	0.01	0.01	−0.01	0	0.11	0.01	0.01	−0.01
B_x	−0.03	0.00[c]	0.21	0.10	0.17	∼−0.06	0.01[c]	0.02	0.01	0.06
B_y	−0.21	−0.31[c]	−0.18	−0.15	−0.07	∼−0.06	−0.10[c]	−0.07[c]	−0.10	0.01
B_x-B_y	0.18	0.31	0.39	0.25	0.24	∼−0.0	0.09	0.09	0.11	0.05

[a] The sign of *J* is chosen such that the forbidden state is of lower energy if $J > 0$. [b] The energy difference in going from P_1TA to P_2TA or from $P_1TA\text{-}O_2$ to $P_2TA\text{-}O_2$. [c] After correction for resonance, likely errors ±0.1 eV.

The calculated exciton couplings between the excited states derive from underlying couplings between the key molecular orbitals involved in the transitions, the orbitals of the Gouterman four-orbital model. Previously,[7,11] we have examined the coupling between these orbitals in detail, obtaining evidence supporting the principle that *cross-conjugated π-localized systems such as the quinonoid bridge facilitate much weaker coupling than do through-conjugated π-delocalized systems such as the benzenoid bridge*. The large reduction in exciton coupling associated with quinonoid transformation observed herein provides specific experimental verification of this principle.

One noteworthy difference between the observed and calculated exciton couplings is the calculations all predict that the coupling of the B_y band of $P_2TA\text{-}O_2$ is greatly reduced compared to that of P_2TA but not eliminated whereas no residual coupling is apparent experimentally. The remnant calculated coupling is not experimentally verified in this system, but its origin may be very important for other systems. While orbital localization in general reduces coupling, specific orbital effects are also important, and the calculations predict[11] that an accidental bridge ($3b_{2g}$) to chromophore ($4b_{3g}$) resonance interaction maintains the coupling between the porphyrin LUMO orbitals and is manifest through the calculated residual B_y exciton coupling.

Our primary interest here is in the use of oligoporphyrins in molecular electronic devices. These are more likely to employ electron or hole transport through coupled molecular orbitals, as modeled earlier,[7,11] rather than exciton transport through coupled excited states, as investigated experimentally herein. Experiments which directly access electron or hole transport, particularly in continuously conducting devices, are rare and difficult, whereas electronic absorption spectra of key component systems are readily obtained. However, the current continuous device can readily be related to orbital couplings;[1,5,6,48] hence, in this work we have shown how it is possible to extract key molecular electronic properties from the spectra, leading to a new paradigm useful in the construction of such devices, chemically controlled molecular switches. Note that, while in practice the direct chemical interconversion of the benzenoid and quinonoid forms TA and $TA\text{-}O_2$ of the bridges are impractical, chemical species containing related motifs are readily interconvertible. Studies are underway in our laboratory investigating the photochemical, chemical, and electrochemical interconversion of the porphyrin-appended quinone $P_2TA\text{-}O_2$, and its reduced hydroquinone form $P_2TA\text{-}(OH)_2$, as are investigations of similar reactions of the analogous dioxime (═NOH replacing ═O).[49] Such molecules may find application in new sensing, control, and high-capacity memory technologies.

Acknowledgment. We thank the Australian Research Council for financial support for this work.

JA020081U

(48) Datta, S. *Electronic transport in mesoscopic systems*; Cambridge University Press: Cambridge, 1995.
(49) Crossley, M. J.; Johnson, L. A. Unpublished results.
(50) Kim, B. F.; Bohandy, J. *J. Mol. Spectrosc.* **1978**, *73*, 332.
(51) Nagashima, U.; Takada, T.; Ohno, K. *J. Chem. Phys.* **1986**, *85*, 4524.
(52) Rimington, C.; Mason, S. F.; Kennard, O. *Specrochim. Acta* **1958**, *12*, 65.